Numerical Investigation of the Effects of Loading and Slot Harmonics on the Core Losses of Induction Machines

E. Dlala[1], O. Bottauscio[2], M. Chiampi[3], M. Zucca[2], A. Belahcen[1] and A. Arkkio[1]
[1] Aalto University School of Science and Technology, FI-00076 Aalto, Finland
[2] Istituto Nazionale di Ricerca Metrologica (INRIM), Turin, I-10135, Italy
[3] Politecnico di Torino, Turin, I-10129, Italy
Email: emad.dlala@aalto.fi

***Abstract*—This paper aims to investigate core losses in induction motors running under different loading conditions. The investigation is conducted using 2-D finite-element methods incorporating two different core-loss models. The simulation results show that the core losses increase significantly with loading and the effect of slot harmonics on the eddy-current loss and minor loops can be remarkable.**

I. Introduction

Electrical machines dissipate power losses under no-load and loading conditions. It is well understood that increasing the load leads to a remarkable rise in copper losses. On the other hand, it is widely misunderstood that increasing the load leads to a *drop* in the core losses. The assumption that core losses decrease by increasing the load evolved originally from the prominent T equivalent circuit by which the core losses are computed as a function of the voltage over the shunt resistance.

Although it is true that the total flux in the core of an electrical machine decreases by increasing the load, the subsequent calculation of core losses by the equivalent circuit is not correct. The total flux decreases because of the voltage drop occurring over the stator resistance and the leakage flux taking place at the end-windings. Usually, slotting, saturation, rotor motion and the driving circuit generate harmonic ripple in the machine under no-load and full-load conditions. However, the shape and distribution of the fluxes change dramatically with loading, leading to an overall increase in the harmonic content and an overall decrease in the amplitude of the fundamental flux components. Therefore, even though the fundamental flux components decrease by increasing the load, the core losses will increase as a result of the increase in the flux distortions and higher harmonics [1]–[4].

In the conventional calculations of power losses in electrical machines, usually, a compensating vague term named as "stray load loss" is added as a function of the load in order to compensate for the additional losses generated by the higher harmonics in the stator and the rotor. Such calculation, however, produces a gross estimation of the losses because stray load loss is defined in the Standards as that portion of losses that is not accounted for by the sum of core loss, stator and rotor resistive losses, and friction and windage losses. The vagueness of this definition has left many manufacturing companies of electrical machines struggling how to deal with the core losses. In this paper, however, we will not focus particularly on the fundamental concept of stray load loss, but we rather aim to use the finite-element method (FEM) to investigate the effects of loading on core losses of two squirrel-cage induction motors.

II. Methods of Analysis

A. FE Governing Equations

Performing a 2-D approach over the solution region results in the following:

$$-\nabla \cdot (\nu \, \nabla A) + \sigma \frac{\partial A}{\partial t} = J_{\mathrm{s}} \tag{1}$$

where ν is the nonlinear magnetic reluctivity, σ is the electrical conductivity, t is the time, A and J_{s} are the z-components of the magnetic vector potential and the electric current density, respectively. The resulting 2-D FEM equations are coupled with the circuit equations of the stator windings. The rotor circuit (end-ring) is also included in the analysis. The skin effect is modeled in the rotor cage but not in the stator filamentary conductors [5]. The motion of the rotor is modeled by changing the mesh in the air-gap at each time-step. The overall system of equations is discretized in time and solved iteratively using the Newton Raphson method.

B. Core-Loss Computation

In the following, two different approaches for computing the core losses are used as a posteriori. In both approaches, the characterization of losses is considered through the prediction of the three well-known power loss components: hysteresis, P_{hy}, excess, P_{ex}, and eddy-current, P_{cl}, losses.

1) Simplified Approach: Using this approach, the eddy-current loss is computed using the classical approach under the assumption that the flux is uniform and independent of the material characteristics (no skin-effect). The hysteresis and excess losses are computed in the absence of minor loops based on the method proposed in [6]:

$$\begin{aligned} P_{\mathrm{hy}} &= P_{\mathrm{h,max}} + P_{\mathrm{h,min}}[R(\hat{B}_{\mathrm{max}}) - 1] \\ P_{\mathrm{ex}} &= P_{\mathrm{e,max}} + P_{\mathrm{e,min}}[R(\hat{B}_{\mathrm{max}}) - 1] \end{aligned} \tag{2}$$

where $P_{\mathrm{h,max}}$, $P_{\mathrm{h,min}}$, $P_{\mathrm{e,max}}$ and $P_{\mathrm{e,min}}$ are, respectively, the static and excess power losses calculated along the orthogonal directions defined by the major B_{max} and minor B_{min} axes of the flux density ellipse [7]. $\hat{B}_{\mathrm{max}}$ is the peak of B_{max}. The

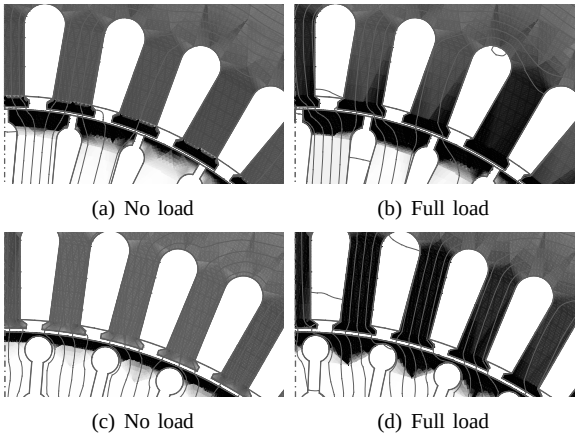

(a) No load (b) Full load

(c) No load (d) Full load

Fig. 1. Distribution of the core losses computed by the advanced model for the 15-kW motor (top) and the 37-kW motor (bottom). Same scale was used in the plots. The darker the color is the higher density of loss.

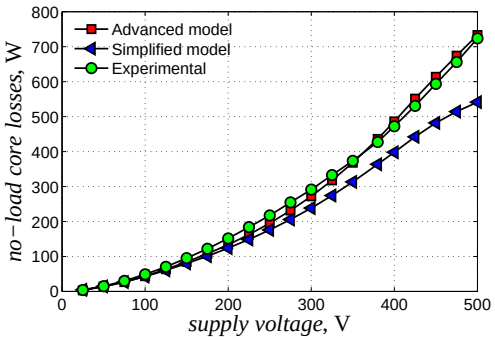

Fig. 2. No-load core losses of the 37-kW motor computed by FEM and compared with experiments.

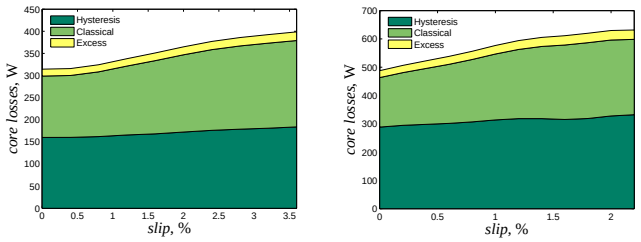

(a) 15-kW motor (b) 37-kW motor

Fig. 3. Core losses computed by the advanced model at different slips.

correction function R is deduced by experiments on material samples magnetized under alternating and rotating fluxes. The static loss P_{h} is obtained from measurements performed on Epstein strips using alternating flux density of different peak values and the excess loss P_{e} is computed based on the statistical theory of losses [4].

2) High-Accuracy Advanced Approach: Using this approach, the magnetodynamic eddy-current problem is solved using two coupled 1-D penetration equations derived from Maxwell's laws in which the edge effects are neglected

$$\frac{\partial^2 H_x(z,t)}{\partial z^2} = \sigma \frac{\partial B_x(z,t)}{\partial t} \tag{3}$$

$$\frac{\partial^2 H_y(z,t)}{\partial z^2} = \sigma \frac{\partial B_y(z,t)}{\partial t} \tag{4}$$

where z is the axis of the lamination depth, perpendicular to the magnetic field that rotates in the x-y plane. The time-dependent equations (3) and (4) are formulated using a two-component magnetic vector potential, discretized by FEM, and solved iteratively using the fixed-point method [5]. The hysteretic and viscosity effects are taken into account using a dynamic vector Preisach model.

III. Results

The core losses have been simulated and investigated under various loading conditions for two 4-pole, 50-Hz, 380-V induction motors of different shaft powers (15 kW and 37 kW) and different rotor-cage topologies (see Fig. 1). The core-loss models are first validated by experiments performed on the motors at no load with different operating voltage levels (see Fig. 2). The results of the advanced model showed excellent agreement with the experimental results in the whole voltage range. The results of the simplified approach showed reasonable agreement up till the rated voltage. At higher voltages, however, the influence of skin-effect and the inaccuracies in estimating hysteresis losses become more pronounced.

Simulations carried out for the motors at different slips are shown in Fig. 3. The 15-kW motor has a rotor-cage with semi-open slots while the 37-kW motor has a deep-bar rotor with closed slots. At no load, the 37-kW machine generates less harmonic ripple because minor changes occur in the reluctance of the magnetic path at the airgap during the movement of the rotor. At full load, when the machine draws more current, the iron in the closed-slot side saturates because of the magnetic field generated in the rotor. Such a behavior is affirmed by the change in the loss density shown in Fig. 1 between the no-load case and full-load case.

References

[1] A. M. Knight and Yang Zhan, "Identification of flux density harmonics and resulting iron losses in induction machines with nonsinusoidal supplies," *IEEE Trans. Magn.*, v. 44, pp. 1562-1565, 2008.

[2] J. Seo, T. Chung, C. Lee, S. Jung, and H. Jung, "Harmonic iron loss analysis of electrical machines for high-speed operation considering driving condition," *IEEE Trans. Magn.*, v. 45, pp. 4656-4659, 2009.

[3] K. Yamazaki and N. Fukushima, "Iron-loss modeling for rotating machines: comparison between Bertotti's three-term expression and 3-D eddy-current analysis," *IEEE Trans. Magn.*, v. 46, pp. 3121-3124, 2010.

[4] O. Bottauscio, M. Chiampi, A. Manzin, and M. Zucca, "Prediction of losses in induction machines: a challenge for the modelling approach," *Eur. Phys. J. Appl. Phys.*, v. 30, pp. 7-16, 2005.

[5] E. Dlala, "Comparison of models for estimating magnetic core losses in electrical machines using the finite-element method," *IEEE Trans. Magn.*, v. 45, pp. 716-725, 2009.

[6] F. Fiorillo, "Characterization of losses in electrical steels," *EU Brite Euram*, Tech. Rep. Project no. BRPR950 019, 1996-1998.

[7] O. Bottauscio, A. Canova, M. Chiampi, and M. Repetto, "Iron losses in electrical machines: influence of different material models," *IEEE Trans. Magn.*, v. 38, pp. 805-808, 2002.